Tutorial

Del Vecchio, A; Holobar, A; Falla, D; Felici, F; Enoka, R M; Farina, D

Link to publication on Research at Birmingham portal

1   **Tutorial: Analysis of motor unit discharge characteristics from high-density surface EMG**
2   **signals**

3

4   A. Del Vecchio[1], A. Holobar[2], D. Falla[3], F. Felici[5], R. M. Enoka[4], D. Farina[1]

5   **Affiliations:**

6   [1]Department of Bioengineering, Imperial College London, SW7 2AZ, London, UK.

7   [2]Faculty of Electrical Engineering and Computer Science, University of Maribor, Koroška cesta 46,

8   2000 Maribor, Slovenia

9   [3]Centre of Precision Rehabilitation for Spinal Pain (CPR Spine), School of Sport, Exercise and

10   Rehabilitation Sciences, College of Life and Environmental Sciences, University of Birmingham,

11   Birmingham, UK

12   [4]Department of Integrative Physiology, University of Colorado Boulder, Colorado

13   [5]Department of Movement, Human and Health Sciences, University of Rome "Foro Italico", Rome,

14   Italy.

15   **Corresponding author:**

16   Dario Farina. Department of Bioengineering, Imperial College London, SW7 2AZ, London, UK. Tel:

17   Tel: +44 (0)20 759 41387, Email: d.farina@imperial.ac.uk

20

21

22

23

24

25

26

Abstract

Recent work demonstrated that it is possible to identify motor unit discharge times from high-density surface EMG (HDEMG) decomposition. Since then, the number of studies that use HDEMG decomposition for motor unit investigations has increased considerably. Although HDEMG decomposition is a semi-automatic process, the analysis and interpretation of the motor unit pulse trains requires a thorough inspection of the output of the decomposition result. Here, we report guidelines to perform an accurate extraction of motor unit discharge times and interpretation of the signals. This tutorial includes a discussion of the differences between the extraction of global EMG signal features versus the identification of motor unit activity for physiological investigations followed by a comprehensive guide on how to acquire, inspect, and decompose HDEMG signals, and robust extraction of motor unit discharge characteristics.

Introduction

The generation of movement is accomplished by the transmission of synaptic inputs to motoneuron pools. The transducer of synaptic input into forces is the motor unit, which comprises a group of muscle fibres (muscle unit) and an alpha motor neuron. The neural information is transmitted by the motor unit through axonal action potentials (neural drive to the muscle) that elicit action potentials in the innervated muscle unit (motor unit action potentials, Figure 1). The summation and time-course of the motor unit action potentials determine the characteristics of the surface electromyogram (EMG) recorded with electrodes placed on the skin during motor tasks (Day and Hulliger, 2001; Fuglevand et al., 1992; Heckman and Enoka, 2012; Milner-Brown et al., 1973). The shapes of the surface-recorded motor unit action potentials are influenced by the properties of the volume conductor (Dimitrov and Dimitrova, 1974; Enoka and Duchateau, 2015; Farina et al., 2002b; Mañanas et al., 2016; Merletti et al., 2003; Stegeman et al., 1997).

Due to the physiological safety factor at the neuromuscular junction, the identification of motor unit action potentials from the interference EMG signals informs us about the discharge activity of individual motoneurons (Desmedt and Godaux, 1977; Duchateau and Enoka, 2011; Enoka and Duchateau, 2015; Gandevia et al., 1990; Henneman et al., 1965; Milner-Brown et al., 1973; Milner-Brown and Stein, 1975). Based on this approach, the motoneuron is the only nerve cell that can be noninvasively recorded in humans. For these reasons, several surface EMG decomposition methods have been proposed over the past three decades (Chen et al., 2018; Chen and Zhou, 2016; De Luca et al., 2006; Farina et al., 2010; Gazzoni et al., 2004; Holobar et al., 2014; Holobar and Zazula, 2007; Kumar et al., 2020; Nawab et al., 2010; Negro et al., 2016a). Of these methods, in this tutorial we focus exclusively on those based on blind source separation (BSS) methods applied to high-density surface EMG.

Over the past two decades, non-invasive high-density surface EMG (HDEMG) electrodes have been used to identify motor unit discharge times (Drost et al., 2001; Farina et al., 2002a; Gazzoni et al., 2005; Masuda and De Luca, 1991; Merletti et al., 2008, 1999; Zwarts and Stegeman, 2003). These recordings provide a spatial sampling of the motor unit action potentials at the skin surface (Holobar et

65 al., 2010; Merletti and Farina, 2016; Negro et al., 2016a; Zwarts and Stegeman, 2003). From these
66 recordings, blind source separation (BSS) procedures can identify motor unit discharge times (Chen
67 and Zhou, 2016; Holobar et al., 2010; Negro et al., 2016a) during a range of isometric tasks (A Del
68 Vecchio et al., 2019c; Gallego et al., 2015; Martinez-Valdes et al., 2017). Although BSS decomposition
69 procedures are performed in an automatic way, they require user-inspection of the identified motor unit
70 spike trains (Enoka, 2019).

71 The aim of this tutorial article is to provide guidelines for the decomposition of HDEMG recordings.
72 Moreover, we discuss the limits, the potential, and how to further validate the results obtained with
73 HDEMG decomposition. The future advances needed in EMG decomposition are also discussed, with
74 an emphasis on the computational challenges required to remove the subjectivity during visual editing
75 of the motor unit spike trains.

76

77 **1 – Extracting neural information from high-density EMG signals: Global EMG estimates vs.**
78 **decomposition**

79 Since the surface EMG signal is the algebraic summation of motor unit action potentials (Day and
80 Hulliger, 2001), it is influenced by both the discharge times and the waveforms of the action potentials
81 of the active motor units (Figure 1).
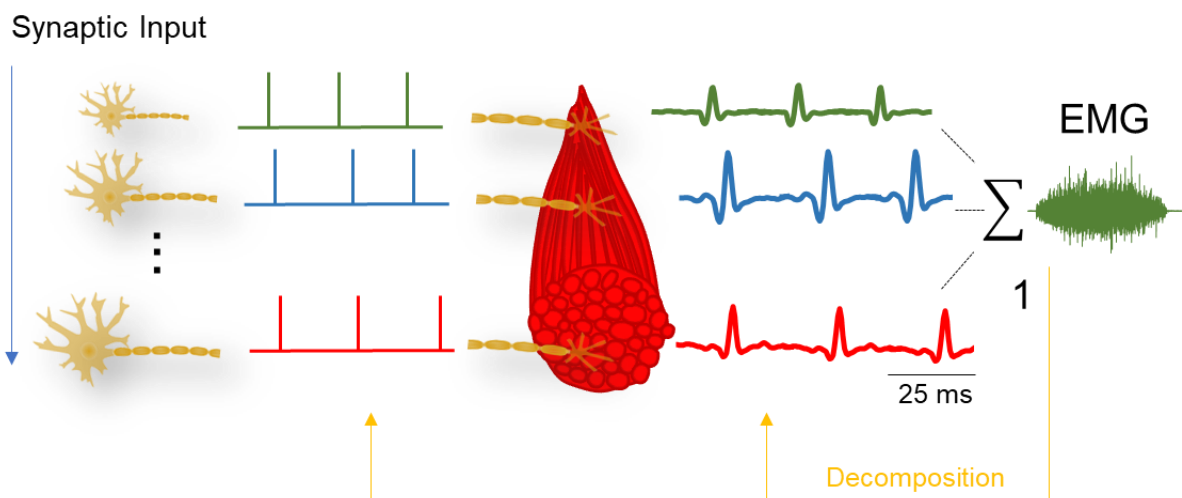
82

83 **Figure 1** The one-to-one correspondence between axonal action potentials and motor unit action
84 potentials. A pool of motoneurons discharges a series of action potentials (left) that are transformed by
85 the muscle unit in a time series of motor unit action potentials (right). The motor unit action potential
86 vary in amplitude and these differences are not always associated with the size of the motor unit, due
87 to the influence of the volume conductor. The summation of the motor unit action potentials corresponds
88 to the recorded EMG signals. Due to these effects, the association between the strength of the neural
89 drive to the muscle and EMG amplitude is not always linear. Rather, the neural drive to the muscles
90 can only be estimated from the motor unit discharge times, such as by decomposition of high-density
91 surface EMG recordings (line 1 in orange). Conversely, conventional EMG analyses often estimate the
92 neural drive to the muscle by extracting global features of the signal, such as amplitude or spectral
93 moments. The decomposition of the EMG signal identifies the series of action potentials for individual
94 motor units (red spikes). Due to several limitations with the global EMG, however, it is not always correct
95 to infer the motoneuron population activity from global EMG signals, for example, because of the effects
96 of amplitude cancellation and the non-linear relation between action potential sizes and recruitment
97 thresholds. *Note that the innervation zones of the motoneurons are shown in largely different positions

98　of the muscle only to improve figure clarity while often the innervation zones are clustered in relatively
99　small muscle portion.

100　The characteristics of the motor unit action potentials depend on many factors; for example, action
101　potential amplitude and conduction velocity, which scale with the diameter of the muscle fibre
102　(Håkansson, 1956; Plonsey and Barr, 1988). The amplitude of the motor unit action potentials also
103　depends on the number of innervated muscle fibres, which is associated to the motor unit recruitment
104　threshold (the voluntary force level corresponding to the first discharge of a motor unit) (Milner-Brown
105　and Stein, 1975). However, this association is confounded by the influence of the volume conductor
106　and, therefore, by the distance between the muscle fibres and the recording electrodes (Besomi et al.,
107　2019) Consequently, the association between recruitment threshold and motor unit action potential
108　amplitude is usually weak (Del Vecchio et al., 2017; Keenan et al., 2006), which influences the
109　associations between EMG amplitude and the strength of the neural drive to the muscle and between
110　EMG amplitude and force (Del Vecchio et al., 2017; Dideriksen et al., 2011; Fuglevand et al., 1993;
111　Keenan et al., 2006; Komi and Viitasalo, 1976). It also makes it challenging to compare EMG amplitude
112　across subjects, muscles, and time (Besomi et al., 2019).

113　Experimental results on the association between the amplitude of motor unit action potentials and motor
114　unit size, which are consistent with simulation results of EMG generation (Farina et al., 2014), indicate
115　that the amplitude of the EMG is only a crude indicator of the neural strategies used to control muscle
116　force (Enoka, 2019; Enoka and Duchateau, 2015). Figure 2, for example, shows that the amplitude of
117　the action potential waveforms for three motor units can be unrelated to the recruitment thresholds (Del
118　Vecchio et al., 2017).

A Tibialis anterior myoelectrical activity during an increasing force contraction

2000 (μV)

1 (s)

B

a.u

C Motor unit discharge times + Spike triggered average

D Single motor unit action potential propagating in the matrix

E Low threshold motor unit

F High threshold motor unit

a.u

25 (ms)

Recruitment Threshold = 24.9 (%)	6.19 (%)	63.9 (%)
Conduction Velocity = 4.41 (m/s)	3.82 (m/s)	5.20 (m/s)
Median Frequency = 147.80 (Hz)	120.95 (Hz)	124.07 (Hz)
Root mean square = 248.06 (μV)	115.75 (μV)	143.45 (μV)

119

Figure 2 Association between motor unit action potential properties and recruitment threshold. **A** Eight double-differential EMG signals of the tibialis anterior muscle during an isometric ankle-dorsiflexion contraction at up to 70% of maximal voluntary force at a rate of 5% MVC/s (thick black trace). **B** 500 ms of EMG activity for the 8 channels. **C** Motor unit action potentials were identified by EMG decomposition and spike-triggered averaging. **D-E-F** Three representative motor unit action potentials with recruitment thresholds 24.9, 6.2, and 63.9 % of maximal force. The estimated conduction velocity, root mean square amplitude, and mean power spectral frequency are also shown for each motor unit action potential. (a.u = arbitrary units, scaled amplitude of the EMG). Reproduced with permission from Del Vecchio et al. (2017).

120   Contrary to surface action potential amplitude, the estimated conduction velocity of the motor unit action

121   potentials has been shown to be associated with motor unit recruitment threshold across subjects and

122   muscles, and to be influenced by different types of training interventions (Andreassen and Arendt-

123   Nielsen, 1987; Casolo et al., 2019; Del Vecchio et al., 2017; Gazzoni et al., 2005; Martinez-Valdes et

124   al., 2018; Masuda et al., 1996; Masuda and De Luca, 1991; Zwarts and Arendt-Nielsen, 1988). The

125   conduction velocity estimated from the global EMG signal is the weighted average of the motor unit

126   conduction velocities.

127   Due to the challenges associated with interpreting the features extracted from the surface EMG (Del

128   Vecchio et al., 2017; Farina et al., 2014, 2004), intramuscular (LeFever et al., 1982; LeFever and De

129   Luca, 1982; McGill et al., 2005; Stashuk and de Bruin, 1988) and surface EMG decomposition methods

130   have been proposed (Chen et al., 2018; Chen and Zhou, 2016; De Luca et al., 2006; Farina et al., 2010;

131   Gazzoni et al., 2004; Holobar et al., 2014; Holobar and Zazula, 2007; Nawab et al., 2010; Negro et al.,

132   2016a). These methods identify individual motor unit action potentials during voluntary contractions

133   and, therefore, allow the comparison of motor unit properties across subjects and time. Moreover, the

134   same motor unit can be tracked over time (Del Vecchio and Farina, 2019; Martinez-Valdes et al., 2017)

135   and compared across sessions including before and after training interventions (A Del Vecchio et al.,

136   2019a; Martinez-Valdes et al., 2018). In contrast to global EMG analysis, the identification of the

137   discharge times of individual motor units provides a direct estimate of the neural drive to muscle.

138   As an example of the information that can be obtained when decomposing EMG signals with respect

139   to global analysis, we recently showed that the activity of motoneurons identified by EMG decomposition

140   is predictive of the maximal rate of force development (A Del Vecchio et al., 2019c). Similarly, the

141   detrimental influence of aging on force steadiness was shown to be associated with the variability in the

142   common synaptic input to motoneurons, as estimated by EMG decomposition (Feeney et al., 2018).

143   Researchers now have a new tool to observe the neural code for movement in humans directly with a

144   non-invasive approach that can be used in a variety of conditions. Nonetheless, surface EMG

145   decomposition must be used carefully and requires expertise in signal acquisition, interpretation of

146   results, and manual assessment of decomposition quality. After testing the validity of HDEMG

147   decomposition algorithms in several methodological studies (e.g., Holobar *et al.*, 2010, 2014; Marateb

148   *et al.*, 2011; Negro *et al.*, 2016*a*; Del Vecchio & Farina, 2019*a*), here we now share guidelines on how

149   to perform HDEMG decomposition by BSS accurately and how to identify motor unit properties reliably.

150

151   **2 - High-density surface EMG signals: acquisition**

152   Prior to applying the high-density electrode grids (Figure 2C), the skin should be shaved, lightly

153   abraded, and cleansed with an alcoholic solution and with abrasive paste (Piervirgili et al., 2014).

154   Source separation is based on the assumption that action potential waveforms of motor units are unique

155   when recorded by the grid. Therefore, the EMG electrodes should be placed in a location that assures

156   maximal variations in shape of the action potentials of different motor units. For example, when

157   recording from fusiform muscles, it is preferable to position the EMG array with its centre approximately

158   above a primary innervation zone. In other types of muscles (e.g., pennate muscles) the BSS is less
159   sensitive to the position of the electrode array, although the electrodes will still need to be placed over
160   the muscle belly. Interestingly, these requirements for decomposition are opposite to those often
161   discussed for extracting global features from the EMG (Barbero et al., 2012).

162   The interelectrode distances used for HDEMG usually range from 3-4 mm to 10 mm (Drost et al., 2001;
163   Merletti and Muceli, 2019; Zwarts and Stegeman, 2003; Del Vecchio et al., 2018; Farina et al., 2010;
164   Feeney et al., 2018; Gazzoni et al., 2005; Holobar et al., 2010; Negro et al., 2016a). It should be noted
165   that the electrode array does not need to satisfy the requirement for spatial Nyquist sampling frequency
166   for successful BSS. Whether or not the spatial Nyquist criterion needs to be met depends on how the
167   decomposition results will be used; for example, high spatial sampling may be necessary when
168   analysing the spatial distribution of the identified motor unit action potentials (Merletti and Muceli, 2019).
169   Therefore, the choice of the interelectrode distance is usually dictated by practical criteria, such as the
170   size of the muscle.

171   After the electrode grids are applied, the signals should be assessed for quality. This should preferably
172   be done by displaying the signals as monopolar recordings, as these signals are the most sensitive to
173   interference. The visual inspection of monopolar signals allows the operator to find and remove the
174   sources contaminating the recordings. The monopolar derivation is usually the most sensitive to signal
175   interferences and therefore poses the highest constraints on signal quality, whereas the bipolar
176   derivation better reveals the short-circuited EMG channels and also their spatial diversity. When the
177   main sources of EMG signals are located at greater distances, it is not uncommon to observe EMG
178   signals with high amplitudes in monopolar derivation but small amplitudes in bipolar derivation, because
179   of the filtering of common spatial signal components by the bipolar system. In such cases, the spatial
180   variation across different EMG channels is substantially reduced, effectively decreasing the number of
181   useful EMG channels and, thus, the yield of BSS techniques. Accepted baseline noise levels for
182   HDEMG signals are in the order of $10 - 40$ µV RMS, but this requirement may vary with contraction
183   intensity. From empirical experience, at low EMG amplitudes signal noise should be no more than one
184   half of the power of the signal to ensure reliable decomposition (Del Vecchio et al., 2017; A Del Vecchio
185   et al., 2019a). Aside from the electrode-skin and electronic-amplification noise (signal noise), EMG
186   decomposition can only identify relatively few active motor units. The activity of the unidentified motor
187   units is an additional, and often the main, source of noise for the decomposition process.

188   The EMG signals are usually band-pass filtered between 10-20 Hz at the low end and 400-500 Hz at
189   the high end. This range keeps most of the EMG signal power while filtering out the contributions of
190   signal noise. The decomposition process will be influenced by the choice of filter settings as this may
191   alter the action potential waveforms. In general, the smaller the bandwidth, the greater the similarity of
192   action potentials for different motor units. However, a smaller bandwidth does decrease the level of
193   noise. The use of zero-phase filters, when possible, is recommended to avoid variable delays
194   introduced for action potentials of different motor units and to keep the energy of motor unit action
195   potentials concentrated in short intervals of time. Nonlinear filtering techniques change the EMG mixing
196   model and should be avoided.

Noise may differ across channels and it may be necessary to remove some channels from the analysis.
Among the methods that can be used to identify channels with low signal-to-noise ratio, one approach
is to check the quality of the signal by estimating the power spectral density for each electrode in the
grid and comparing it with the baseline. Figure 3 shows an example of 63 (from a total of 64) signals
with high signal-to-noise ratio and shows how channels with poor signal quality can be identified. After
having identified the electrodes showing high signal-to-noise ratio, potential power line interferences
can be removed with filtering techniques (e.g., notch filters). Similar considerations apply for notch filters
as for the choice of the bandpass filters discussed above.

After the EMG signal quality check, visual confirmation, and filtering of the EMG signals, the BSS
decomposition can be initiated.
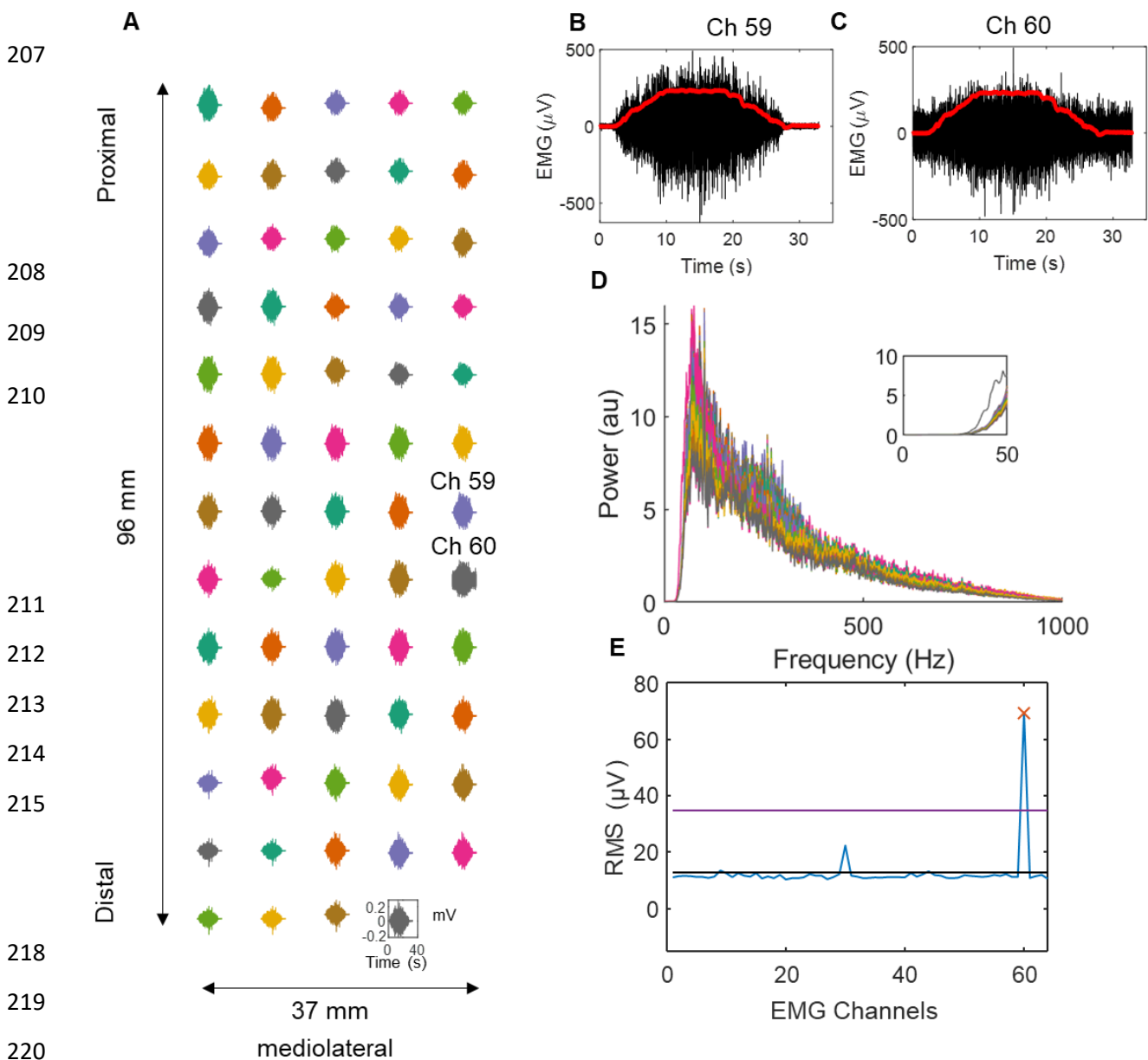
Figure 3 Example of detection and visual display of channels with poor signal-to-noise ratio. **A** Sixty-
four monopolar EMG signals from the tibialis anterior muscle during a contraction at 35% of maximal

force. Two signals (channel 59 and 60) are highlighted and displayed in **B.** The force trace is indicated
by the red lines. The 60th channel shown in **C** has a high level of noise at baseline, as it can be seen
from its power spectral density (**D**) and from the baseline amplitude of the EMG. **D.** The power spectral
density of each of the 64 channels, as computed from the full contraction duration (~24 s). Note that
one channel (in the inset, grey line) shows higher power at lower frequencies than all the others. This
indicates poor signal-to-noise ratio (channel 60, au for auxiliary units) **E.** Three standard deviations from
the EMG root mean square (RMS) baseline across the grid shows the outlier channel.

3 - High-density surface EMG signals: decomposition

High-density EMG signals are decomposed into individual motor unit action potentials with methods
that have limited a-priori information. Figure 4 shows an overview of the decomposition process:
acquisition of HDEMG recordings, separation of sources (motor units) via BSS, visual inspection, and
raster plot of the reliably identified motor units. BSS procedures usually estimate one motor unit spike
train at a time by iteratively optimizing the motor unit separation filter and applying it to the recorded
EMG signals. Importantly, optimization of the motor unit filter builds on a measure of sparseness for the
motor unit spike train based on a predefined time interval. Different measures of spike-train sparseness
have been proposed (Chen and Zhou, 2016; Holobar and Zazula, 2007; Negro et al., 2016a), but they
all require relatively long EMG recordings for the spike train to be estimated reliably. Consequently,
current BSS algorithms should be applied to EMG signals that last at least 5 s.
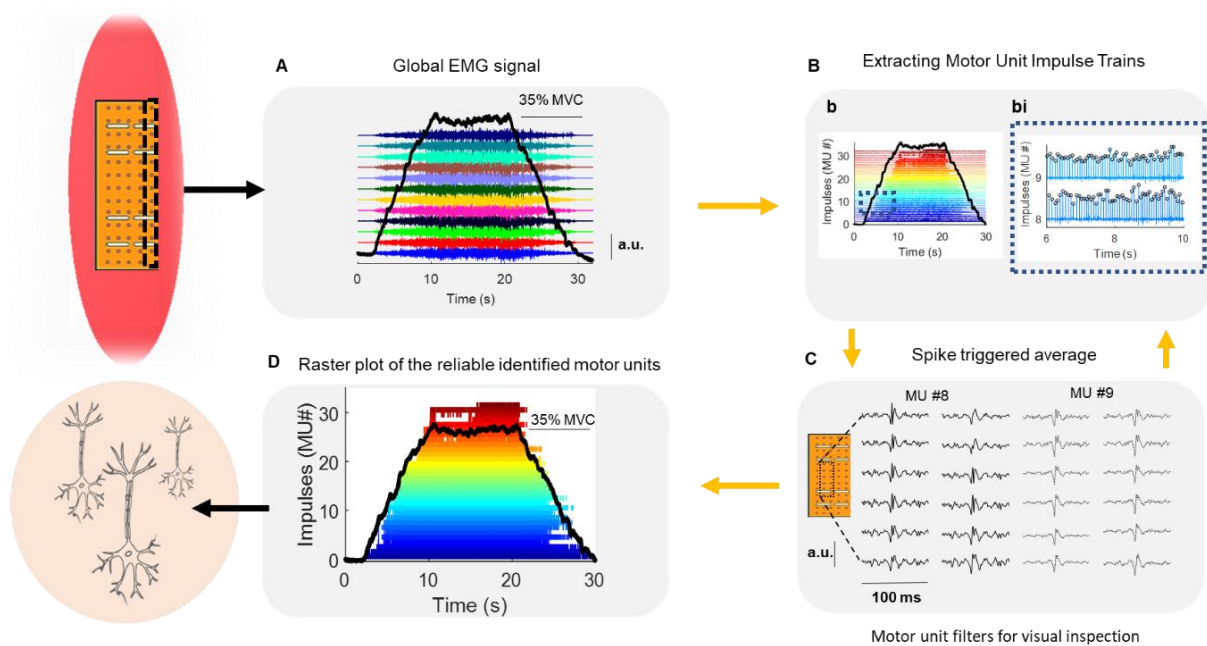
Figure 4 Example of high-density surface EMG decomposition with blind-source separation and visual
inspection of the signals. **A**. Tibialis anterior monopolar EMG activity during an isometric contraction.
The rate of force development was 5% MVC/s with a plateau phase of 10 s. One column of the high-
density EMG grid (64 electrodes in total, with 8 mm of interelectrode distance, au arbitrary units) is
shown color-coded. Specifically, the channels highlighted by the dotted black trace (over the muscle,
left side of the figure) are shown in **A**. In this example, the signal-to-noise ratio is similar for all 64
electrodes in the matrix. **B.** Extraction of motor unit pulse trains by blind-source separation. The 64
channels are decomposed blindly, and the output of the algorithm are impulse trains with heights
corresponding to the weights of the motor unit action potential shapes in the matrix obtained by the

253 independent component analysis process. The two insets in B (b and bi) show the motor unit impulses
254 extracted by blind-source separation for each motor unit. The next iteration is to check each motor unit
255 action potential visually, as shown in **bi**, and reiterate the source separation manually by triggering the
256 motor unit action potential in a fixed time window, usually in the order of 3-5 s, as shown in **bi** and **C**.
257 After visual inspection of all the motor unit spike trains, it is possible to observe the raster plot of all
258 identified motor units (**D**). The motor unit waveforms in **C** represents the motor unit waveforms
259 corresponding to 12 electrodes after spike-triggered averaging.

260

261 4 - High-density surface EMG signals: visual inspection of decomposition results

262 Due to the sparseness of the motor unit spike train, BSS calculates the motor unit separation filter from

263 those time instants in the EMG recording when the motor unit was likely to be active. Once the motor

264 unit spike train is identified, the motor unit filter can be re-calculated based only on the identified motor

265 unit spikes, in an iterative way. This can be accomplished by inspecting the results of the BSS algorithm,

266 so that the operator can manually identify and remove from the calculation of the separation filter the

267 spikes of lower quality. Note that this partly manual selection is for the calculation of the separation filter

268 only and not for the output of the decomposition (see also below). This selection can often improve the

269 motor unit separation filter estimates beyond the level achieved by the BSS algorithm used fully

270 automatically. For example, when decomposing EMG signals that contain artefacts, the BSS algorithm

271 will try to optimize the motor unit filter on all the motor unit spikes, including those occurring concurrently

272 with artefacts. It is exactly this noise and the residual activity of the other motor units that is measured

273 by some signal-based metrics of accuracy, such as the pulse-to-noise ratio (Holobar et al., 2014).

274 Under assumption of nonstationary noise and artefacts, following the initial automatic decomposition it

275 is always possible to identify the portions of a spike train with low pulse-to-noise ratio and exclude those

276 portions from the motor unit filter calculation. It is not a simple matter to implement the exclusion of the

277 low-quality portions of the motor unit spike train automatically in a BSS algorithm. Indeed, the pulse-to-

278 noise ratio (and therefore the quality of spike train portions) may change due to many factors such as

279 the contraction level (increase of contraction level increases the contributions of other motor units),

280 changes of skin-electrode contact noise, instrument noise, and signal artefacts. The human operator

281 builds on the knowledge of the experimental protocol and currently can decide which signal intervals to

282 exclude from the motor unit filter optimization better than a BSS algorithm, which has no knowledge on

283 the experimental conditions.

284 After exclusion of spike-train intervals with poor signal quality, the motor unit filter should be re-
285 calculated and re-applied to the entire EMG signal in order to re-estimate (objectively, without any
286 manual intervention) the entire motor unit spike train. An example of this procedure if shown in Figure
287 5.
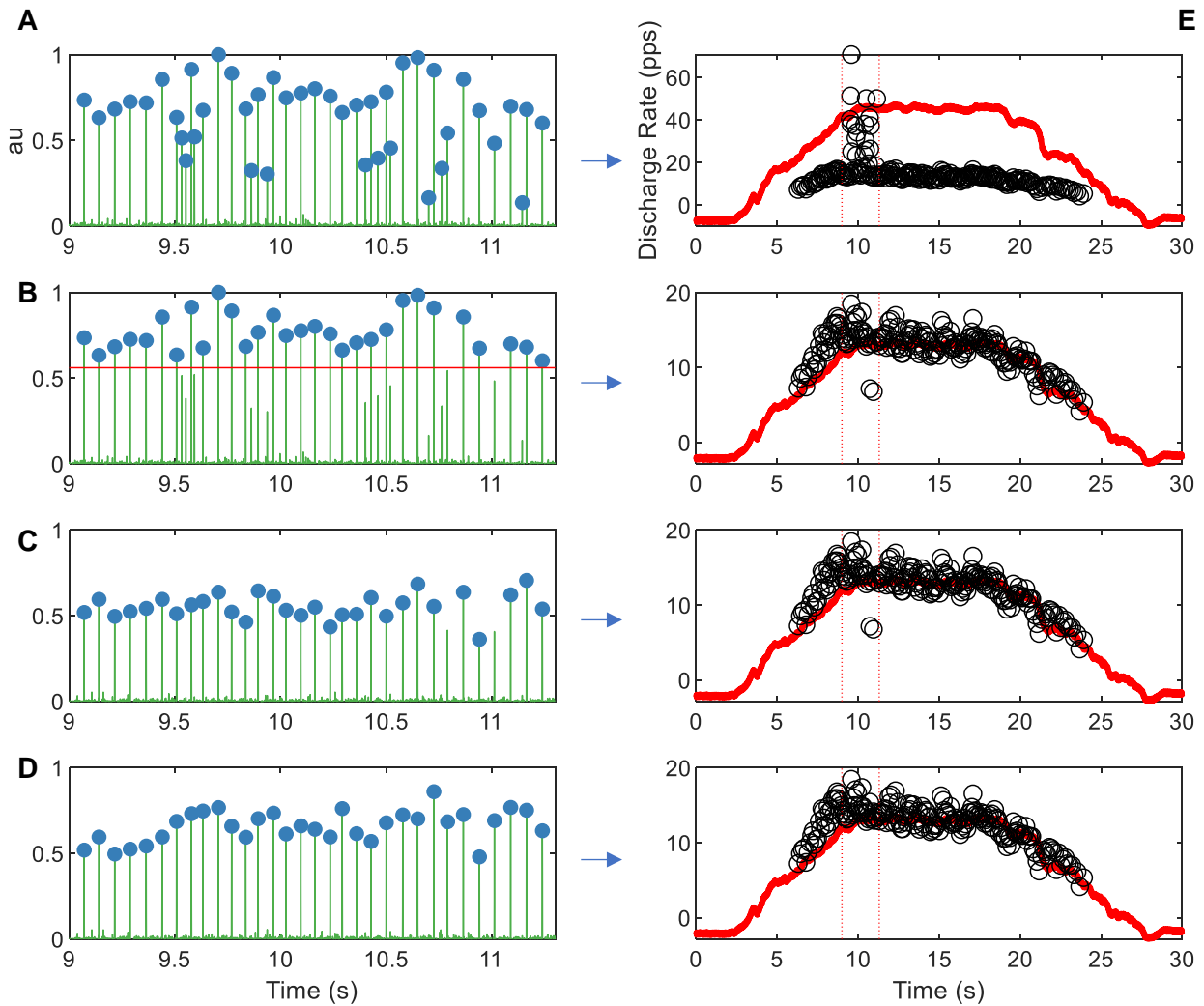
288

Figure 5. Visual reiterations of the motor unit discharge times identified by blind source separation (**A-D**). The blind source separation automatically identified the discharge times of a motor unit. In **A**, the left plot depicts the identified spike train with many spikes below the average spike height. Automatically identified motor unit firings are depicted by blue circles. The discharge times of the motor unit (right plot) show a strong mismatch with the average motor unit discharge rate and force trace in red. In these instances, a time window of ~3 s is centred in the location of interest (red dashed lines in **E**). Within this location, the motor unit filter is reconstructed after removing the firings below a certain threshold, as depicted in **B.** The motor unit filter is then reapplied to the HDEMG signals, yielding a new spike train estimate that is depicted in **C**. Afterwards, two more spikes are recognized as motor unit firings and manually added in **D.** In this way, the motor unit filter that was identified by blind source separation is visually edited and yields a robust estimate of the motor unit firings.

289

290

291 Manual exclusion of spike-train intervals in manual optimization of the motor unit filter may or may not
292 rely on the human knowledge of motor unit firing regularity. Although this additional information may be
293 beneficial, it may also bias the selection of motor unit spikes that are taken into consideration when
294 manually re-calculating motor unit filters. Importantly, manual spike selection should only be used for
295 motor unit filter optimization. Afterwards, manually optimized motor unit filters should be applied to the
296 entire EMG signal and objective spike segmentation procedures need to be followed to discriminate
297 spikes from baseline noise in the identified motor unit spike train. Subjective selection of motor unit
298 spikes in the final motor unit spike train (final decomposition result) should be avoided as it may lead to
299 biasing the decomposition results.

300

301 **5 - High-density surface EMG signals: decomposition accuracy**

302 The extraction of motor unit action potentials from high-density EMG signals has been extensively
303 validated, but mainly during isometric contractions. The current accepted approach for the validation of
304 surface EMG decomposition is a variant of the two-source method previously introduced by Mambrito
305 & De Luca (1984) for intramuscular EMG decomposition. With this method, intramuscular and HDEMG
306 signals are concurrently recorded and the results of their decomposition compared (Holobar et al., 2014,
307 2010; Hu et al., 2014; Marateb et al., 2011). Figure 6 shows a raster plot of motor units concurrently
308 identified from surface and intramuscular signals, with the respective accuracies.
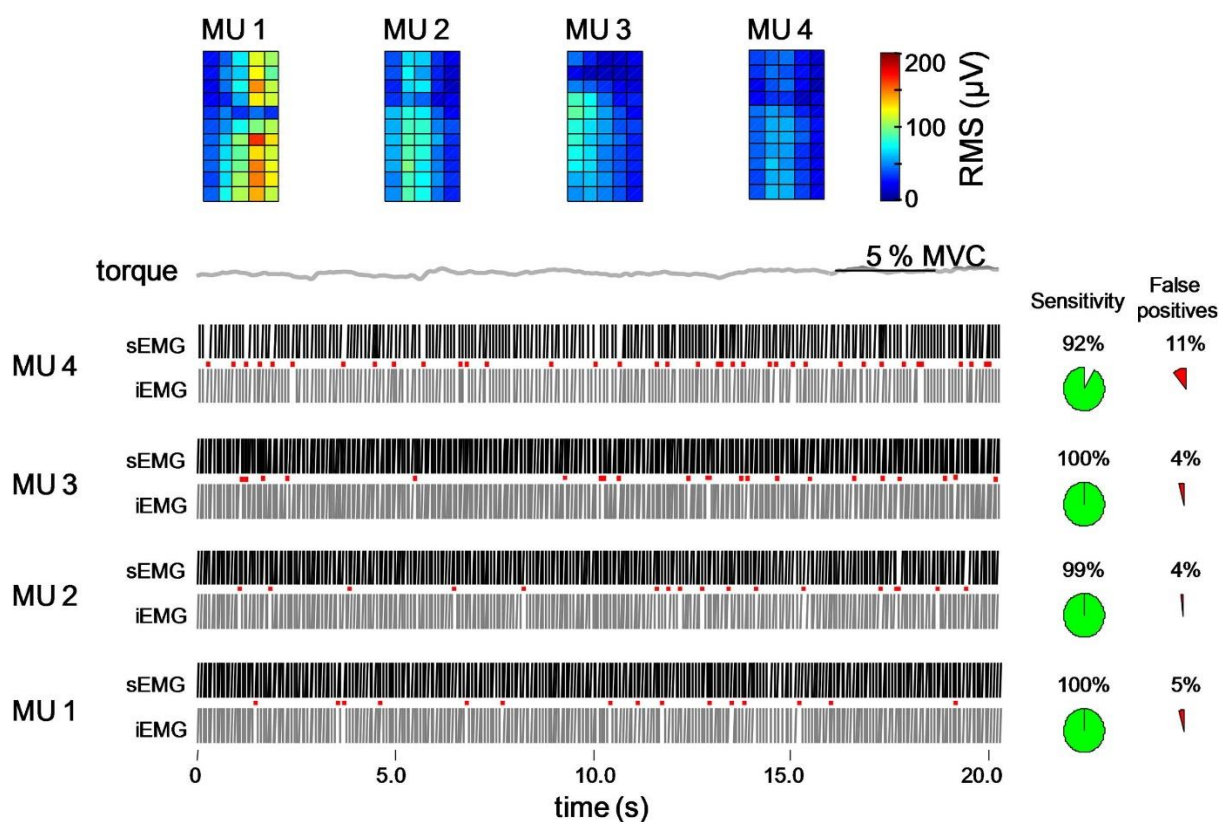
309

310 **Figure 6** Two-source method to assess accuracy. The intramuscular electromyogram(iEMG) is
311 recorded concurrently with high-density surface EMG (sEMG) from the abductor digiti minimi muscle at
312 5% of the maximal voluntary contraction. The sensitivity and false positive rate for discharge time

313 identification are computed by comparing the output of intramuscular and surface EMG decomposition.
314 In this example, the bottom raster plot shows the motor unit discharge times that were identified from
315 the intramuscular EMG signal decomposition and, at the top, those identified by blind-source separation
316 of the HDEMG signals. The top plot in each pair shows the distribution of amplitude of the motor unit
317 action potential waveforms over the high-density EMG grid. The sensitivity of the high-density EMG
318 (right) represents the number of discharge times that are concurrently identified by the surface and
319 intramuscular EMG decomposition divided by the total number of discharges identified from the
320 intramuscular EMG. The percent of false positives corresponds to the number of discharges identified
321 by the surface but not by the intramuscular EMG decomposition, divided by the total number of
322 discharges identified from the intramuscular EMG. MU, motor unit. Reproduced with permission from
323 Farina et al. 2010.

324 Indirect methods of validating surface EMG decomposition use shape analysis of two-dimensional
325 motor unit action potentials identified by BSS (Del Vecchio and Farina, 2019; Hu et al., 2015, 2013a;
326 Thompson et al., 2018) and simulation approaches (Farina et al., 2010; Holobar and Zazula, 2007). For
327 example, accuracy measures, such as pulse-to-noise ratio (Holobar et al., 2014), the silhouette
328 measure (Negro et al., 2016a), or the motor unit action potential similarity after spike-triggered
329 averaging (see below) across the contractions with or without injection of gaussian noise (Del Vecchio
330 and Farina, 2019; Thompson et al., 2018), can be used to infer the accuracy of motor unit spike
331 identification. All of these measures are asymptotic and increase their precision with the number of
332 identified spikes in the spike train. Therefore, they should not be used to assess the accuracy of spike
333 trains with less than 30 spikes (Holobar et al., 2014) or to assess the accuracy of each individual spike
334 in a spike train.

335 Some information about accuracy can be obtained from the spike-triggered averaging of EMG signals
336 (Del Vecchio and Farina, 2019; Hu et al., 2015, 2013b; Thompson et al., 2018). With this approach, the
337 discharge times of identified motor units are used as triggers for an average that is accumulated over
338 time intervals of 25 to 100 ms. Due to the possibility that motor unit action potential shapes change
339 during an isometric contraction, a relatively small number of motor unit discharge times should be used
340 in the spike-triggered average. We empirically observed that 3 s to 5 s (~30-100 spikes) are sufficient
341 to robustly extract motor action potential waveforms during sustained and fast isometric contractions (A
342 Del Vecchio et al., 2019c). Also, the reliability of an identified motor unit pool can be examined by
343 identifying the same motor units across days (see *Motor unit Tracking)*.

344 **6 – Assessment of motor unit properties**

345 From the discharge times of identified motor units, the characteristics of the engaged motor units can
346 be identified. One key characteristic is the recruitment threshold, which corresponds to the force when
347 the first motor unit action potential occurs. The ensuing force that is produced by the muscle fibres
348 innervated by the motoneuron (the muscle unit) occurs with a delay that depends on the axonal
349 conduction velocity and on the properties (active and passive) of the muscle fibres. To obtain reliable
350 estimates of recruitment and derecruitment thresholds, subjects must practice performing slow linear
351 ramp contractions.

352 A common approach used to estimate recruitment threshold and to measure the discharge
353 characteristics of motor units is the performance of trapezoidal force trajectories with controlled rates
354 of increase and decrease in force (5-20% MVC/s) to a moderate plateau force (35-70% of maximal

force). Given the current limitations in HDEMG decomposition analysis in uniformly sampling motor units across recruitment thresholds, it is best practice to use a range of target forces (30 to 70-90% of maximum force) depending on the test muscle and type of contraction.
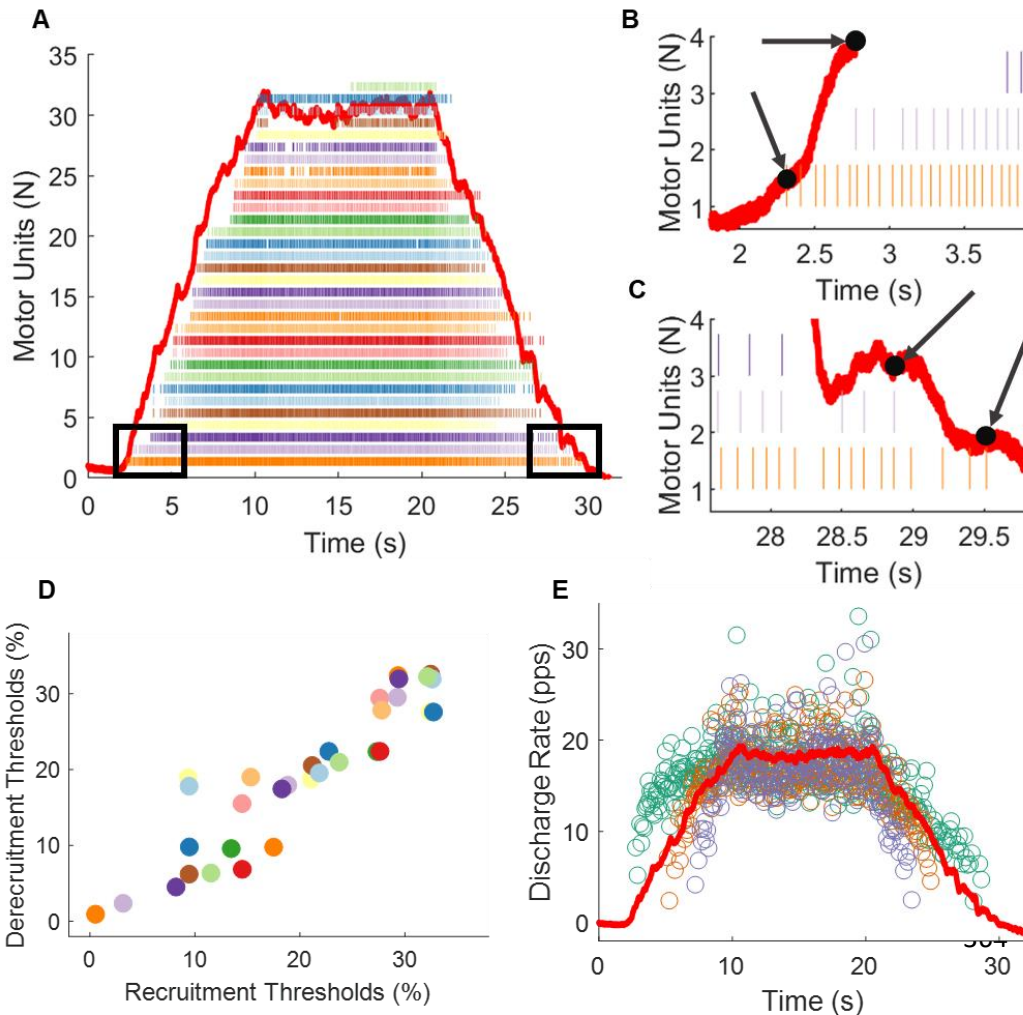

Figure 7. Motor unit properties: recruitment thresholds and discharge rates during an isometric trapezoidal contraction (plateau 35% of maximum). **A**. Raster plot of 32 identified motor units during an isometric contraction of the tibialis anterior muscle. The black boxes highlight the recruitment (**B**) and derecruitment (**C**) phases for three motor units with the specific force indicated with a black arrow. **D.** The association between recruitment threshold and derecruitment thresholds. **E**. The instantaneous discharge rate (the inverse of the interspike interval) as a function of time for the three representative motor units. The force trace is in red colour.

Figure 7 shows the raster plot of discharge times of 32 motor units during a trapezoidal contraction up to 35% of the maximum force of the tibialis anterior muscle. The recruitment and derecruitment thresholds are highlighted in Figure 7A-C. Once the interspike intervals are known, the motor unit discharge rates can be determined during the recruitment, plateau, and derecruitment phases, as shown in Figure 7E for three representative motor units.

372   Estimates of motor unit recruitment threshold during fast contractions can provide a measure of the

373   speed of recruitment (Fig. 8).

374
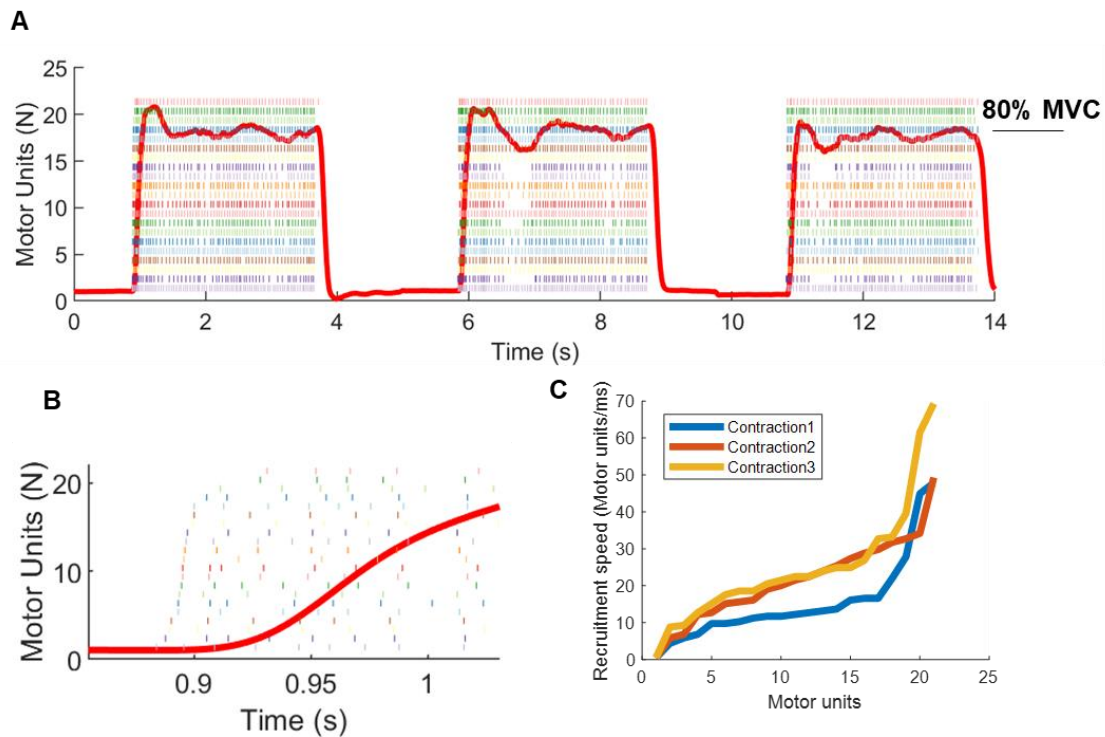
375

Figure 8 Motor unit recruitment during fast contractions. **A**. Three rapid isometric contractions of the tibialis anterior muscle. The plateau of the force is ~80% of maximum (red-trace). **B**. One representative contraction during the first 100 ms. The discharge times of identified motor units are shown as tick marks. **C**. Motor unit recruitment speed represents the time interval between the first discharge times of consecutive motor units (B). This value is calculated by taking the average of the derivative of the first discharge times of the motor unit pool (sorted by recruitment order). The x-axis label in C is sorted with respect to the motor units showing the smallest time interval. In this example, all the identified motor units were recruited in a small time window (<50 motor units/ms).

376

377

378   From the discharge times of the motor units, it is possible to extract characteristics of the common

379   synaptic input to the motoneuron pool. These measures can be obtained in both the time and frequency

380   domain. One time domain approach is to compute the cross-correlogram between motor unit discharges

381   (Nordstrom et al., 1992). This method, originally proposed for pairs of motor units, can be extended to

382   populations of motoneurons by summing the motor unit spike trains (binary signal) to generate the

383   cumulative spike trains (CST). The cross-correlogram is then performed between the CSTs of randomly

384   permuted groups of motor units (Figure 9). The rate of increase in correlation between CSTs when the

385   number of motor units used for the CST calculation increases is associated to the relative proportion of

386   common input with respect to independent input. This proportion can also be quantified by non-linear

387   fitting of the peak correlation values in the frequency domain (Negro et al., 2016b), or in the time domain.

388   These estimates provide information on a bandwidth of motor neuron input that depends on the filtering

of the CSTs. For example, by using a Hanning window of 25-ms (A Del Vecchio et al., 2019b), the

390   analysed bandwidth is approximately 40 Hz.

391

392
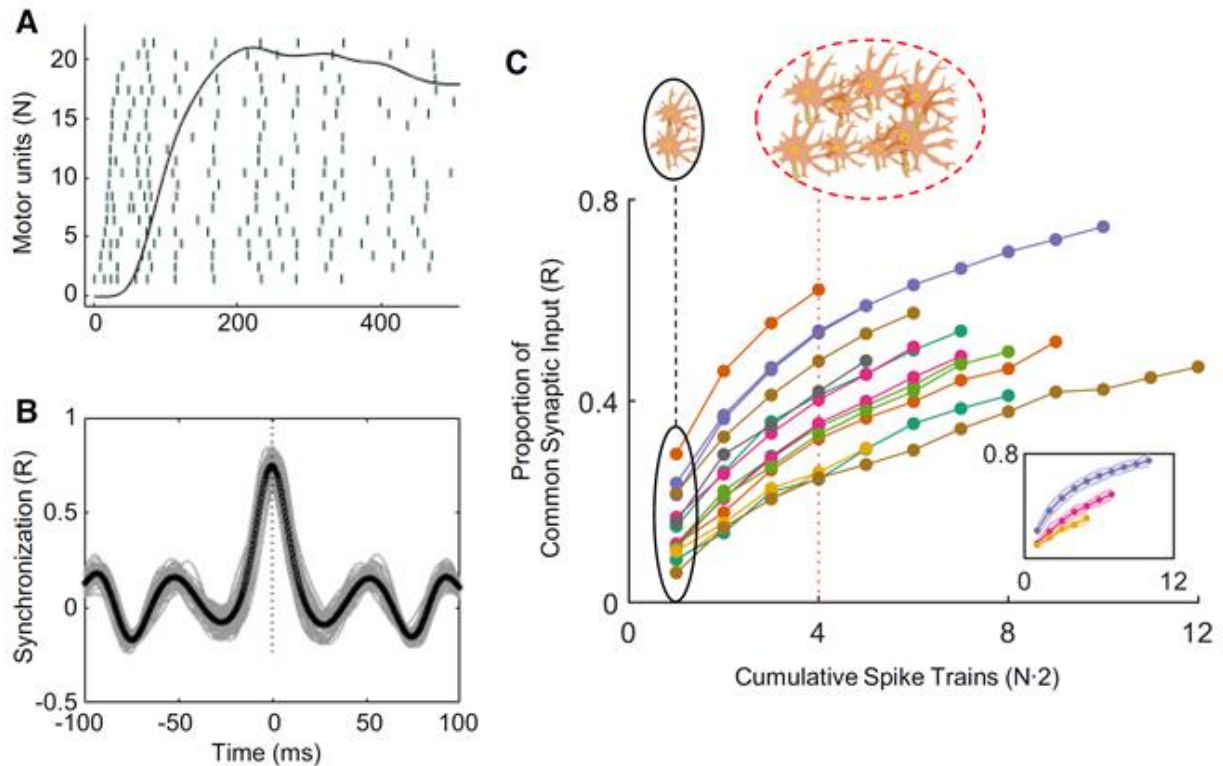
Figure 9. Calculation of the proportion of common input from the cross-correlogram. **A** Raster plot of
21 motor units during a fast contraction. **B** The cross-correlogram was obtained in 100-ms time windows
with a 5-ms overlap. Each shaded grey line corresponds to a time window. For each calculation, the
motor unit spike trains were divided in two equally sized groups and convolved with a 25-ms Hanning
window. **C** Individual subject data (color-coded) for the strength of correlation between CSTs as a
function of the number of motor units used for each CST. The inset in C shows three representative
subjects with standard deviation across three rapid contractions (shaded colour). Modified from Del
Vecchio et al. 2019 with permission.

401

402   It is further possible to estimate the frequency bands of the input shared by motoneurons (in the

403   assumption of an approximate linear input-output relation for the motoneuron population) during steady

404   contractions that last at least 20-30 s with the use of coherence functions. The coherence function

405   provides a cross-correlation analysis in the frequency domain. Figure 10 shows the procedure for this

406   calculation. Only motor unit spike trains without silent periods (>500 ms) should be included in this

407   analysis. The coherence function can be also applied to study the shared synaptic inputs within the

408   discharge timings of the populations of motoneurons. For this purpose, the coherence function is

409   applied to groups of motor units that belong to different muscles, as described previously (Del Vecchio

410   et al., 2019; Laine et al., 2015).

411   Another information that can be extracted from the motor unit discharge times is an estimate of the

412   strength of persistent inward currents (PICs) to motoneurones from the discharge rates at recruitment

413   and derecruitment (Gorassini et al., 2002; Heckman et al., 2005). This measure reflects
414   neuromodulatory input received by motoneurones and has been recently performed from HDEMG
415   signal decomposition (Hassan et al., 2020).

416   From the shape of the motor unit action potential waveform it is also possible to extract other
417   physiological information. This information includes analysis of the motor unit waveform, such as
418   amplitude and conduction velocity (see paragraph 1-2 and Figure 2). The analysis of the motor unit
419   discharge times and action potential waveforms enables the analysis of neural and peripheral properties
420   concurrently. For example, the strong association between motor unit recruitment thresholds and motor
421   unit conduction velocities that have been reported for different muscles (Andreassen and Arendt-
422   Nielsen, 1987; Del Vecchio et al., 2018; Hogrel, 2003; Masuda and De Luca, 1991) is consistent with
423   the size principle. Although in some cases this information has been used to infer the type of recruited
424   (fast-twitch or slow twitch) muscle fibres, in-vivo studies show that there is no clustering of conduction
425   velocity values but rather a continuous distribution of conduction velocities and estimated muscle fibre
426   diameters (Del Vecchio et al., 2018; Troni et al., 1983), which agrees with basic physiological studies
427   (see Enoka et al., 2015 for review).
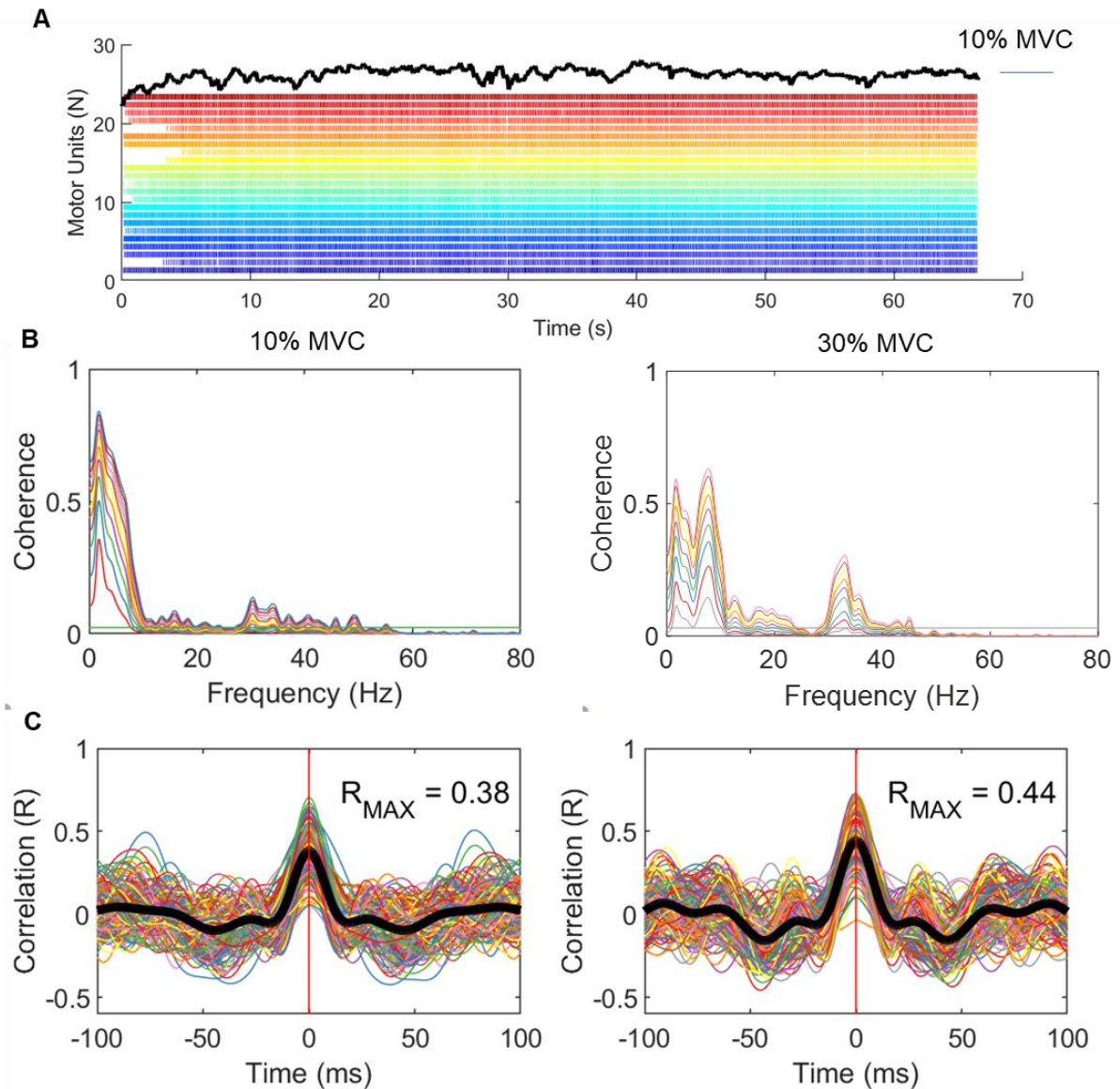
Figure 10 A. Raster plot of motor unit discharge times from the tibialis anterior muscle during a steady contraction at 10% of maximal voluntary force. **B.** The coherence function was calculated between increasing numbers of motor units (color coded) for a contraction at 10 and one at 30% of the maximum. Note that the increase in the number of motor units corresponds to an increase in the frequency coupling in all frequency bands above significance (the significant level was computed as the maximal value of coherence above 100 Hz). **C**. The correlation in the time domain obtained by the cross-correlogram in 100-ms windows.
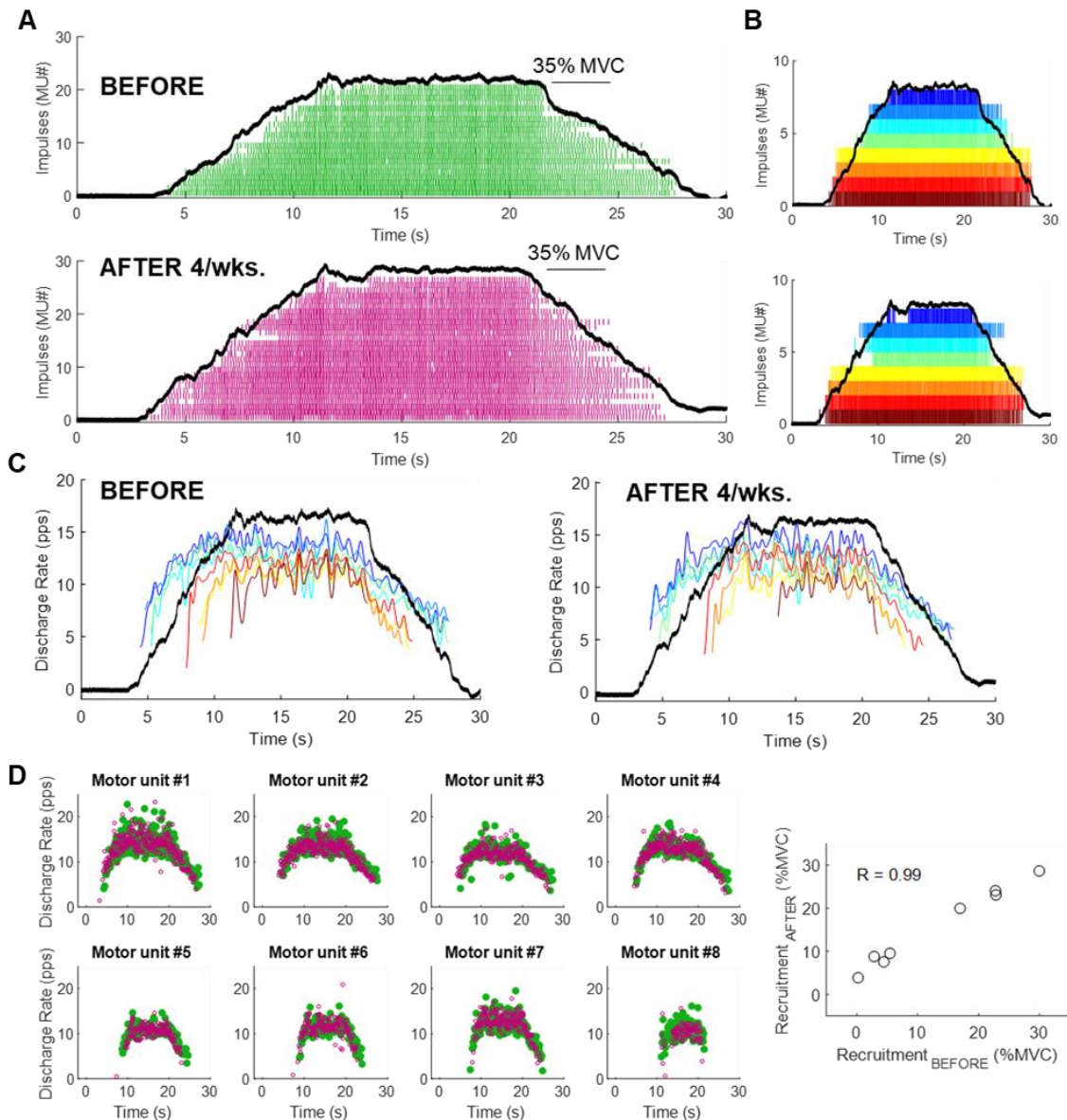
7 - Motor unit tracking

The comparison of motor unit properties during longitudinal studies, such as after a rehabilitation intervention, is only possible if the same motor unit can be identified before and after the intervention. One advantage of HDEMG recordings is that they usually provide high spatial resolution of the motor unit action potentials. There is a small likelihood that two motor units would show exactly the same action potential waveforms in all channels for a large electrode grid (Farina et al., 2008), which means that motor units can be tracked over multiple sessions when the grid is placed in a similar location in each session (Del Vecchio and Farina, 2019; Martinez-Valdes et al., 2017).

443   Figure 11 shows an example of motor unit tracking during an isometric contraction with the ankle
444   dorsiflexors. In this example, only some of the identified motor units could be tracked across
445   experimental sessions. In our experience, approximately 30% of the identified units can be tracked over
446   weeks in the tibialis anterior muscle. Motor unit tracking requires consistent placement of the high-
447   density grid and the establishment of a threshold in cross-correlation between motor unit action
448   potentials. When multiple motor units have a high cross-correlation between each other, which happens
449   occasionally, these motor units should be removed from the tracking (see Figure 3 in (A Del Vecchio et
450   al., 2019a)).

451   The motor unit tracking technique can also be used to test decomposition accuracy. Figure 11 shows
452   two pools of motor units identified during two experimental sessions four weeks apart during isometric
453   trapezoidal contractions of the tibialis anterior muscle. The action potential waveforms of these motor
454   units were used to track the motor units over time (Fig 11B). Once the motor units are tracked, it is
455   possible to test the accuracy and reliability of the discharge characteristics of the motor units, such as
456   discharge rate and recruitment thresholds. Figure 11C-D shows that the tracked motor units exhibited
457   strong reliability in discharge rate and recruitment threshold. It is important to note that the tracking
458   technique uses the 2D action potential waveforms, therefore the physiological properties of the motor
459   units are not taken into account during tracking. It is unlikely that a pool of motor units shows the same
460   discharge characteristics across days (as demonstrated by comparing random motor units across
461   sessions; Martinez-Valdes *et al.*, 2017) if the motor unit tracking and the initial decomposition were not
462   performed correctly (Figure 11).

463

464

Figure 11. *Motor unit tracking.* One method that can be used to assess decomposition accuracy is to track the same motor unit across time. **A.** Two isometric contractions were performed by the same subject with 4 weeks between contractions. The number of identified motor units (green vs purple) differs in the two contractions. **B.** The same motor unit is tracked across time by matching the action potential waveforms**.** Eight motor units that were successfully tracked in the two contractions. Note the similar smoothed discharge rate (**C**), the instantaneous discharge rate (**D**), and the recruitment thresholds (the tracked motor units are color-coded). The scatter plot in **D** shows a strong correlation (P<0.0001) for recruitment thresholds before and after four weeks, thereby underscoring the accuracy in decomposition.

8 – Influencing factors in motor unit decomposition: the influence of muscle, volume conductor, and target force

There are three major limitations that limit the applicability of surface EMG decomposition in some experimental conditions. The output of the decomposition is sensitive to the muscles investigated, the volume conductor properties of the specific subject, and the contraction intensity. These limitations are due to anatomical constraints (the volume conductor between the recording electrodes and the muscle

20

481 units) and superimposition of the muscle fibre action potentials. With increasing contraction forces, the
482 number of motor units that can be identified by decomposition usually decreases. For example, in the
483 tibialis anterior muscle, which is a reliable muscle for decomposition (Del Vecchio and Farina, 2019;
484 Negro et al., 2016a), we observed a 30% reduction in the number of motor units that can be identified
485 when the target force increases from 35% to 70% of maximum force. Similarly, there is a trend for a
486 lower number of identified motor units for subjects with a thicker subcutaneous layer. These trends are
487 due to the decrease in discriminative information in the action potential waveforms of different motor
488 units when the signal bandwidth is reduced by the volume conductor (Farina et al., 2008). There are
489 still not sufficient data to reach a conclusion on the number of identified motor units between sexes.

490

491 Figure 12 shows the number of identified motor unit across muscles, sex, and contraction intensity for
492 a relatively large dataset of decomposed signals collected in the laboratories of the Authors. Some
493 muscles yield higher numbers of motor units irrespective of the contraction intensity (such as tibialis
494 anterior, see Fig 12). We have noted that muscles with fibres that are not all parallel to each other
495 usually yield a greater number of identified motor units by decomposition. This is likely due to the larger
496 discriminative information between motor unit action potentials of different units in muscles with varying
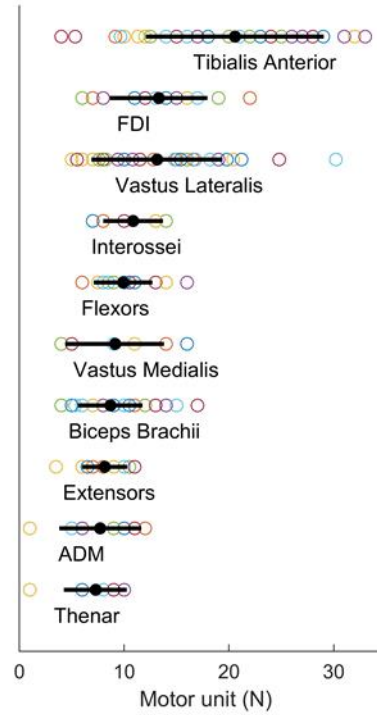497 anatomy.

498

499
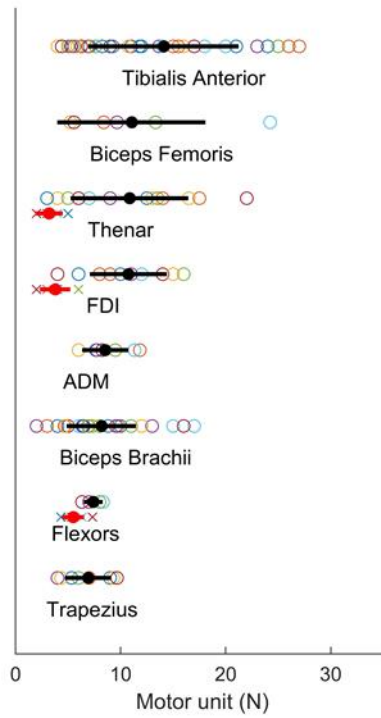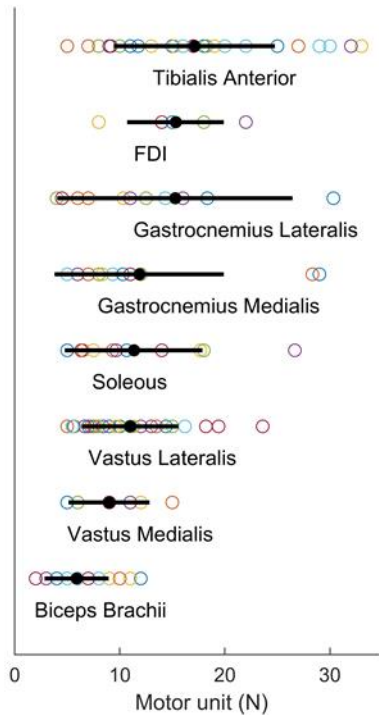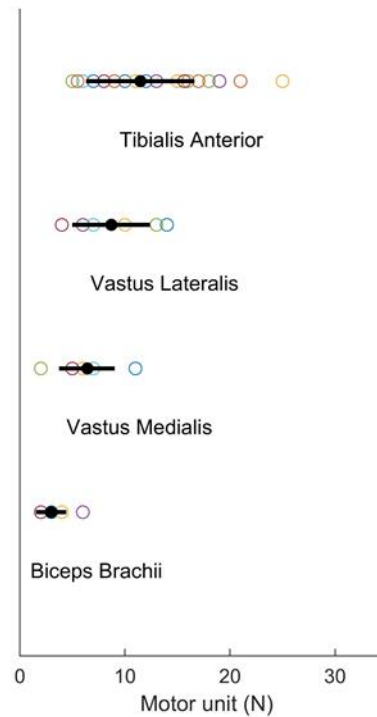
Figure 12 Number of identified motor units across muscles and contraction intensities. The average number (black dots) and standard deviation (black line) across subjects (color-coded), muscles, and contraction intensities. The red line and x dots for three muscles at ≤20% MVC indicate data for women. Note that some muscles yield a greater number of identified motor units irrespective of the contraction intensity. The data shown here are from recordings from the laboratories of the Authors. All the motor

506 units reported in this graph were decomposed with a pulse-to-noise ratio >30dB and were visually
507 inspected as described in this tutorial.

508

509 **Conclusions**

510 In this tutorial we present guidelines for the extraction of motor unit discharge characteristics from

511 HDEMG signals. This article provides an overview of the rationale for decomposition of EMG signals

512 and then describes the step-to-step guidelines on how to perform an accurate decomposition,

513 interpretation, and analysis of motor unit discharge times. Although the advances in software and

514 hardware technology obtained in the last two decades potentially allows any experimenter to record

515 motor units, there are many challenges that need to be overcome and many limitations that need to be

516 solved thorough experimental testing and the development of additional software and hardware. We

517 emphasise that the output of decomposition must be inspected carefully. Moreover, progress is still

518 needed to improve surface EMG decomposition to reduce the limitations associated with variability of

519 performance due to muscle and subject anatomy.

524

525 **Reference**

526 Andreassen, S., Arendt-Nielsen, L., 1987. Muscle fibre conduction velocity in motor units of the
527   human anterior tibial muscle: a new size principle parameter. J. Physiol. 391, 561–571.

528 Barbero, M., Merletti, R., Rainoldi, A., 2012. Atlas of Muscle Innervation Zones, Atlas of Muscle
529   Innervation Zones. https://doi.org/10.1007/978-88-470-2463-2

530 Besomi, M., Hodges, P.W., Van Dieën, J., Carson, R.G., Clancy, E.A., Disselhorst-Klug, C., Holobar,
531   A., Hug, F., Kiernan, M.C., Lowery, M., McGill, K., Merletti, R., Perreault, E., Søgaard, K.,
532   Tucker, K., Besier, T., Enoka, R., Falla, D., Farina, D., Gandevia, S., Rothwell, J.C., Vicenzino,
533   B., Wrigley, T., 2019. Consensus for experimental design in electromyography (CEDE) project:
534   Electrode selection matrix. J. Electromyogr. Kinesiol.
535   https://doi.org/10.1016/j.jelekin.2019.07.008

536 Casolo, A., Farina, D., Falla, D., Bazzucchi, I., Felici, F., Del Vecchio, A., 2019. Strength Training
537   Increases Conduction Velocity of High-Threshold Motor Units. Med. Sci. Sport. Exerc. 1.
538   https://doi.org/10.1249/MSS.0000000000002196

539 Chen, M., Zhang, X., Chen, X., Zhou, P., 2018. Automatic Implementation of Progressive FastICA
540   Peel-Off for High Density Surface EMG Decomposition. IEEE Trans. Neural Syst. Rehabil. Eng.
541   https://doi.org/10.1109/TNSRE.2017.2759664

542 Chen, M., Zhou, P., 2016. A novel framework based on FastICA for high density surface EMG
543   decomposition. IEEE Trans. Neural Syst. Rehabil. Eng. 24, 117–127.
544   https://doi.org/10.1109/TNSRE.2015.2412038

545 Day, S.J., Hulliger, M., 2001. Experimental simulation of cat electromyogram: Evidence for algebraic
546   summation of motor-unit action-potential trains. J. Neurophysiol. 86, 2144–2158.

547 De Luca, C.J., Adam, A., Wotiz, R., Gilmore, L.D., Nawab, S.H., 2006. Decomposition of surface EMG
548   signals. J. Neurophysiol. https://doi.org/10.1152/jn.00009.2006

549 Del Vecchio, A, Casolo, A., Negro, F., Scorcelletti, M., Bazzucchi, I., Enoka, R., Felici, F., Farina, D.,
550   2019a. The increase in muscle force after 4 weeks of strength training is mediated by
551   adaptations in motor unit recruitment and rate coding. J. Physiol. 0, JP277250.
552   https://doi.org/10.1113/JP277250

553 Del Vecchio, A, Falla, D., Felici, F., Farina, D., 2019b. The relative strength of common synaptic input
554   to motor neurons is not a determinant of the maximal rate of force development in humans. J.
555   Appl. Physiol. 127, 205–214. https://doi.org/10.1152/japplphysiol.00139.2019

556 Del Vecchio, A., Farina, D., 2019. Interfacing the neural output of the spinal cord: robust and reliable
557   longitudinal identification of motor neurons in humans. J. Neural Eng. 17, 016003.
558   https://doi.org/10.1088/1741-2552/ab4d05

559 Del Vecchio, A., Germer, C.M., Elias, L.A., Fu, Q., Fine, J., Santello, M., Farina, D., 2019. The human
560   central nervous system transmits common synaptic inputs to distinct motor neuron pools during
561   non-synergistic digit actions. J. Physiol. 597, 5935–5948. https://doi.org/10.1113/JP278623

562 Del Vecchio, A., Negro, F., Felici, F., Farina, D., 2018. Distribution of muscle fibre conduction velocity
563   for representative samples of motor units in the full recruitment range of the tibialis anterior
564   muscle. Acta Physiol. 222, e12930. https://doi.org/10.1111/apha.12930

565 Del Vecchio, A., Negro, F., Felici, F., Farina, D., 2017. Associations between motor unit action
566   potential parameters and surface EMG features. J. Appl. Physiol. 123, 835–843.
567   https://doi.org/10.1152/japplphysiol.00482.2017

568 Del Vecchio, A, Negro, F., Holobar, A., Casolo, A., Folland, J.P., Felici, F., Farina, D., 2019c. You are
569   as fast as your motor neurons: speed of recruitment and maximal discharge of motor neurons
570   determine the maximal rate of force development in humans. J. Physiol. 1–27.
571   https://doi.org/10.1113/JP277396

572 Del Vecchio, A, Ubeda, A., Sartori, M., Azorin, J.M., Felici, F., Farina, D., 2018. Central Nervous
573   System Modulates the Neuromechanical Delay in a Broad Range for the Control of Muscle
574   Force. J. Appl. Physiol. 44, japplphysiol.00135.2018.
575   https://doi.org/10.1152/japplphysiol.00135.2018

576 Desmedt, J.E., Godaux, E., 1977. Fast motor units are not preferentially activated in rapid voluntary
577   contractions in man. Nature 267, 717–9. https://doi.org/10.1038/267717a0

578 Dideriksen, J.L., Enoka, R.M., Farina, D., 2011. Neuromuscular adjustments that constrain
579   submaximal EMG amplitude at task failure of sustained isometric contractions. J. Appl. Physiol.
580   111, 485–494. https://doi.org/10.1152/japplphysiol.00186.2011

581 Dimitrov, G. V., Dimitrova, N.A., 1974. Extracellular potential field of a single striated muscle fibre
582   immersed in anisotropic volume conductor. Electromyogr. Clin. Neurophysiol.

583 Drost, G., Blok, J.H., Stegeman, D.F., van Dijk, J.P., van Engelen, B.G.M., Zwarts, M.J., 2001.
584   Propagation disturbance of motor unit action potentials during transient paresis in generalized
585   myotonia: A high-density surface EMG study. Brain 124, 352–360.
586   https://doi.org/10.1093/brain/124.2.352

587 Duchateau, J., Enoka, R.M., 2011. Human motor unit recordings: Origins and insight into the
588   integrated motor system. Brain Res. 1409, 42–61. https://doi.org/10.1016/j.brainres.2011.06.011

589 Enoka, R.M., 2019. Physiological Validation of the Decomposition of Surface EMG Signals. J.
590   Electromyogr. Kinesiol. https://doi.org/10.1016/j.jelekin.2019.03.010

591 Enoka, R.M., Duchateau, J., 2015. Inappropriate interpretation of surface EMG signals and muscle
592   fiber characteristics impedes understanding of the control of neuromuscular function. J. Appl.
593   Physiol. 119, 1516–1518. https://doi.org/10.1152/japplphysiol.00280.2015

594 Farina, D., Arendt-Nielsen, L., Merletti, R., Graven-Nielsen, T., 2002a. Assessment of single motor
595   unit conduction velocity during sustained contractions of the tibialis anterior muscle with
596   advanced spike triggered averaging. J. Neurosci. Methods 115, 1–12.
597   https://doi.org/10.1016/S0165-0270(01)00510-6

598 Farina, D., Fosci, M., Merletti, R., 2002b. Motor unit recruitment strategies investigated by surface
599   EMG variables. J. Appl. Physiol. 92, 235–247. https://doi.org/11744666

600 Farina, D., Holobar, A., Merletti, R., Enoka, R.M., 2010. Decoding the neural drive to muscles from
601   the surface electromyogram. Clin. Neurophysiol. 121, 1616–1623.
602   https://doi.org/10.1016/j.clinph.2009.10.040

603 Farina, D., Merletti, R., Enoka, R.M., 2014. The extraction of neural strategies from the surface EMG:
604   an update. J. Appl. Physiol. 117, 1215–1230. https://doi.org/10.1152/japplphysiol.01070.2003

605 Farina, D., Merletti, R., Enoka, R.M., 2004. The extraction of neural strategies from the surface EMG.
606   J. Appl. Physiol. 96, 1486–1495. https://doi.org/10.1152/japplphysiol.01070.2003

607 Farina, D., Negro, F., Gazzoni, M., Enoka, R.M., 2008. Detecting the unique representation of motor-
608   unit action potentials in the surface electromyogram. J. Neurophysiol.
609   https://doi.org/10.1152/jn.90219.2008

610 Feeney, D.F., Mani, D., Enoka, R.M., 2018. Variability in common synaptic input to motor neurons
611   modulates both force steadiness and pegboard time in young and older adults. J. Physiol. 596,
612   3793–3806. https://doi.org/10.1113/JP275658

613 Fuglevand, A.J., Winter, D.A., Patla, A.E., 1993. Models of recruitment and rate coding organization in
614   motor-unit pools. J. Neurophysiol. 70, 2470–2488.

615 Fuglevand, A.J., Winter, D.A., Patla, A.E., Stashuk, D., 1992. Detection of motor unit action potentials
616   with surface electrodes: influence of electrode size and spacing. Biol. Cybern.
617   https://doi.org/10.1007/BF00201021

618 Gallego, J.A., Dideriksen, J.L., Holobar, A., Ibanez, J., Glaser, V., Romero, J.P., Benito-Leon, J.,
619   Pons, J.L., Rocon, E., Farina, D., 2015. The Phase Difference Between Neural Drives to
620   Antagonist Muscles in Essential Tremor Is Associated with the Relative Strength of Supraspinal
621   and Afferent Input. J. Neurosci. 35, 8925–8937. https://doi.org/10.1523/JNEUROSCI.0106-
622   15.2015

623 Gandevia, S.C., Macefield, G., Burke, D., Mckenzie, D.K., 1990. Voluntary activation of human motor
624   axons in the absence of muscle afferent feedback: The control of the deafferented hand. Brain
625   113, 1563–1581. https://doi.org/10.1093/brain/113.5.1563

626 Gazzoni, M., Camelia, F., Farina, D., 2005. Conduction velocity of quiscent muscle fibers decreases
627   during sustained contraction. J. Neurophysiol. 94, 387–394.
628   https://doi.org/10.1152/jn.01182.2004.

629 Gazzoni, M., Farina, D., Merletti, R., 2004. A new method for the extraction and classification of single
630   motor unit action potentials from surface EMG signals. J. Neurosci. Methods.
631   https://doi.org/10.1016/j.jneumeth.2004.01.002

632 Gorassini, M., Yang, J.F., Siu, M., Bennett, D.J., 2002. Intrinsic activation of human motoneurons:
633   reduction of motor unit recruitment thresholds by repeated contractions. J. Neurophysiol. 87,
634   1859–1866. https://doi.org/10.1152/jn.00025.2001

635 Håkansson, C.H., 1956. Conduction Velocity and Amplitude of the Action Potential as Related to
636   Circumference in the Isolated Fibre of Frog Muscle. Acta Physiol. Scand. 37, 14–34.
637   https://doi.org/10.1111/j.1748-1716.1956.tb01338.x

638 Hassan, A., Thompson, C.K., Negro, F., Cummings, M., Powers, R.K., Heckman, C.J., Dewald,
639   J.P.A., McPherson, L.M., 2020. Impact of parameter selection on estimates of motoneuron
640   excitability using paired motor unit analysis, in: Journal of Neural Engineering.
641   https://doi.org/10.1088/1741-2552/ab5eda

642 Heckman, C.J., Enoka, R.M., 2012. Motor Unit. Compr. Physiol. 2, 2629–2682.
643   https://doi.org/10.1002/cphy.c100087

644 Heckman, C.J., Gorassini, M.A., Bennett, D.J., 2005. Persistent inward currents in motoneuron
645   dendrites: Implications for motor output. Muscle and Nerve 31, 135–156.
646   https://doi.org/10.1002/mus.20261

647   Henneman, E., Somjen, G., Carpenter, D.O., 1965. Functional Significance of Cell Size in Spinal
648   Motoneurons. J. Neurophysiol. 28, 560–580.

649   Hogrel, J.Y., 2003. Use of surface EMG for studying motor unit recruitment during isometric linear
650   force ramp. J. Electromyogr. Kinesiol. 13, 417–423. https://doi.org/10.1016/S1050-
651   6411(03)00026-9

652   Holobar, A., Minetto, M.A., Botter, A., Negro, F., Farina, D., 2010. Experimental analysis of accuracy
653   in the identification of motor unit spike trains from high-density surface EMG. IEEE Trans. Neural
654   Syst. Rehabil. Eng. 18, 221–229. https://doi.org/10.1109/TNSRE.2010.2041593

655   Holobar, A., Minetto, M.A., Farina, D., 2014. Accurate identification of motor unit discharge patterns
656   from high-density surface EMG and validation with a novel signal-based performance metric. J.
657   Neural Eng. 11, 016008. https://doi.org/10.1088/1741-2560/11/1/016008

658   Holobar, A., Zazula, D., 2007. Multichannel blind source separation using convolution Kernel
659   compensation. IEEE Trans. Signal Process. 55, 4487–4496.
660   https://doi.org/10.1109/TSP.2007.896108

661   Hu, X., Rymer, W.Z., Suresh, N.L., 2014. Motor unit firing rate patterns during voluntary muscle force
662   generation: a simulation study. J. Neural Eng. 11, 26015. https://doi.org/10.1088/1741-
663   2560/11/2/026015

664   Hu, X., Rymer, W.Z., Suresh, N.L., 2013a. Motor unit pool organization examined via spike-triggered
665   averaging of the surface electromyogram. J. Neurophysiol. 110, 1205–20.
666   https://doi.org/10.1152/jn.00301.2012

667   Hu, X., Rymer, W.Z., Suresh, N.L., 2013b. Assessment of validity of a high-yield surface
668   electromyogram decomposition. J. Neuroeng. Rehabil. 10, 1. https://doi.org/10.1186/1743-0003-
669   10-99

670   Hu, X., Suresh, A.K., Rymer, W.Z., Suresh, N.L., 2015. Assessing altered motor unit recruitment
671   patterns in paretic muscles of stroke survivors using surface electromyography. J. Neural Eng.
672   12, 66001. https://doi.org/10.1088/1741-2560/12/6/066001

673   Keenan, K.G., Farina, D., Merletti, R., Enoka, R.M., 2006. Amplitude cancellation reduces the size of
674   motor unit potentials averaged from the surface EMG. J Appl Physiol 100, 1928–1937.
675   https://doi.org/10.1152/japplphysiol.01282.2005

676   Komi, P. V., Viitasalo, J.H.T., 1976. Signal Characteristics of EMG at Different Levels of Muscle
677   Tension. Acta Physiol. Scand. 96, 267–276. https://doi.org/10.1111/j.1748-1716.1976.tb10195.x

678   Kumar, R.I., Mallette, M.M., Cheung, S.S., Stashuk, D.W., Gabriel, D.A., 2020. A method for editing
679   motor unit potential trains obtained by decomposition of surface electromyographic signals. J.
680   Electromyogr. Kinesiol. 50, 102383. https://doi.org/10.1016/j.jelekin.2019.102383

681   Laine, C.M., Martinez-Valdes, E., Falla, D., Mayer, F., Farina, D., 2015. Motor Neuron Pools of
682   Synergistic Thigh Muscles Share Most of Their Synaptic Input. J. Neurosci. 35, 12207–12216.
683   https://doi.org/10.1523/JNEUROSCI.0240-15.2015

684   LeFever, R.S., De Luca, C.J., 1982. A Procedure for Decomposing the Myoelectric Signal Into Its
685   Constituent Action Potentials— Part I: Technique, Theory, and Implementation. IEEE Trans.
686   Biomed. Eng. https://doi.org/10.1109/TBME.1982.324881

687   LeFever, R.S., Xenakis, A.P., De Luca, C.J., 1982. A Procedure for Decomposing the Myoelectric
688   Signal Into Its Constituent Action Potentials— Part II; Execution and Test for Accuracy. IEEE
689   Trans. Biomed. Eng. https://doi.org/10.1109/TBME.1982.324882

690   Mambrito, B., De Luca, C.J., 1984. A technique for the detection, decomposition and analysis of the
691   EMG signal. Electroencephalogr. Clin. Neurophysiol. 58, 175–188. https://doi.org/10.1016/0013-
692   4694(84)90031-2

693   Mañanas, M.A., Rojas-Martínez, M., Alonso, J.F., 2016. Towards the application of HD-EMG
694   decomposition in clinical practice. Clin. Neurophysiol. 127, 2532–2533.
695   https://doi.org/10.1016/j.clinph.2016.02.005

696   Marateb, H.R., McGill, K.C., Holobar, A., Lateva, Z.C., Mansourian, M., Merletti, R., 2011. Accuracy
697   assessment of CKC high-density surface EMG decomposition in biceps femoris muscle. J.
698   Neural Eng. 8. https://doi.org/10.1088/1741-2560/8/6/066002

699   Martinez-Valdes, E., Farina, D., Negro, F., Del Vecchio, A., Falla, D., 2018. Early Motor Unit
700   Conduction Velocity Changes to High-Intensity Interval Training versus Continuous Training.
701   Med. Sci. Sports Exerc. 50, 2339–2350. https://doi.org/10.1249/MSS.0000000000001705

702   Martinez-Valdes, E., Negro, F., Laine, C.M., Falla, D., Mayer, F., Farina, D., 2017. Tracking motor
703   units longitudinally across experimental sessions with high-density surface electromyography. J.
704   Physiol. 595, 1479–1496. https://doi.org/10.1113/JP273662

705   Masuda, T., De Luca, C.J., 1991. Recruitment threshold and muscle fiber conduction velocity of single
706   motor units. J. Electromyogr. Kinesiol. 1, 116–123. https://doi.org/10.1016/1050-6411(91)90005-
707   P

708   Masuda, T., Sadoyama, T., Shiraishi, M., 1996. Dependence of average muscle fibre conduction
709   velocity on voluntary contraction force. J. Electromyogr. Kinesiol. 6, 267–276.
710   https://doi.org/10.1016/S1050-6411(96)00022-3

711   McGill, K.C., Lateva, Z.C., Marateb, H.R., 2005. EMGLAB: An interactive EMG decomposition
712   program. J. Neurosci. Methods 149, 121–133.

713   Merletti, R., Farina, D., 2016. Surface Electromyography: Physiology, Engineering and Applications,
714   Surface Electromyography: Physiology, Engineering and Applications.
715   https://doi.org/10.1002/9781119082934

716   Merletti, R., Farina, D., Gazzoni, M., 2003. The linear electrode array: A useful tool with many
717   applications. J. Electromyogr. Kinesiol. 13, 37–47. https://doi.org/10.1016/S1050-
718   6411(02)00082-2

719   Merletti, R., Farina, D., Granata, A., 1999. Non-invasive assessment of motor unit properties with
720   linear electrode arrays. Electroencephalogr. Clin. Neurophysiol. Suppl. 50, 293–300.

721   Merletti, R., Holobar, A., Farina, D., 2008. Analysis of motor units with high-density surface
722   electromyography. J. Electromyogr. Kinesiol. 18, 879–890.
723   https://doi.org/10.1016/j.jelekin.2008.09.002

724   Merletti, R., Muceli, S., 2019. Tutorial. Surface EMG detection in space and time: Best practices. J.
725   Electromyogr. Kinesiol. 49, 102363. https://doi.org/10.1016/j.jelekin.2019.102363

726   Milner-Brown, H.S., Stein, R.B., 1975. The relation between the surface electromyogram and
727   muscular force. J. Physiol. 246, 549–569. https://doi.org/10.1113/jphysiol.1975.sp010904

728   Milner-Brown, H.S., Stein, R.B., Yemm, R., 1973. The contractile properties of human motor units
729   during voluntary isometric contractions. J. Physiol. 228, 285–306.
730   https://doi.org/10.1113/jphysiol.1973.sp010087

731   Nawab, S.H., Chang, S.S., De Luca, C.J., 2010. High-yield decomposition of surface EMG signals.
732   Clin. Neurophysiol. 121, 1602–1615. https://doi.org/10.1016/j.clinph.2009.11.092

733   Negro, F., Muceli, S., Castronovo, A.M., Holobar, A., Farina, D., 2016a. Multi-channel intramuscular
734   and surface EMG decomposition by convolutive blind source separation. J. Neural Eng. 13,
735   026027. https://doi.org/10.1088/1741-2560/13/2/026027

736   Negro, F., Şükrü Yavuz, U., Farina, D., 2016b. The human motor neuron pools receive a dominant
737   slow-varying common synaptic input. J. Physiol. 0, 1–45. https://doi.org/10.1113/JP271748

738   Nordstrom, M.A., Fuglevand, A.J., Enoka, R.M., 1992. Estimating the strength of common input to
739   human motoneurons from the cross-correlogram. J. Physiol. 453, 547–74.
740   https://doi.org/10.1111/j.1365-2222.2007.02706.x

741   Piervirgili, G., Petracca, F., Merletti, R., 2014. A new method to assess skin treatments for lowering
742   the impedance and noise of individual gelled Ag-AgCl electrodes. Physiol. Meas.
743   https://doi.org/10.1088/0967-3334/35/10/2101

744 Plonsey, R., Barr, R.C., 1988. Bioelectricity: A quantitative Approach, Bioelectricity: A Quantitative
745   Approach. Springer Science & Business Media, New York, NY. https://doi.org/10.1007/978-0-
746   387-48865-3

747 Stashuk, D., de Bruin, H., 1988. Automatic Decomposition of Selective Needle-Detected Myoelectric
748   Signals. IEEE Trans. Biomed. Eng. https://doi.org/10.1109/10.1330

749 Stegeman, D.F., Dumitru, D., King, J.C., Roeleveld, K., 1997. Near- and far-fields: Source
750   characteristics and the conducting medium in neurophysiology. J. Clin. Neurophysiol.
751   https://doi.org/10.1097/00004691-199709000-00009

752 Thompson, C.K., Negro, F., Johnson, M.D., Holmes, M.R., McPherson, L.M., Powers, R.K., Farina,
753   D., Heckman, C.J., 2018. Robust and accurate decoding of motoneuron behaviour and
754   prediction of the resulting force output. J. Physiol. 0, 1–5. https://doi.org/10.1113/JP276153

755 Troni, W., Cantello, R., Rainero, I., 1983. Conduction velocity along human muscle fibers in situ.
756   Neurology 33, 1453–1459. https://doi.org/10.1212/WNL.33.11.1453

757 Zwarts, M.J., Arendt-Nielsen, L., 1988. The influence of force and circulation on average muscle fibre
758   conduction velocity during local muscle fatigue. Eur. J. Appl. Physiol. Occup. Physiol. 58, 278–
759   283. https://doi.org/10.1007/BF00417263

760 Zwarts, M.J., Stegeman, D.F., 2003. Multichannel surface EMG: Basic aspects and clinical utility.
761   Muscle and Nerve 28, 1–17. https://doi.org/10.1002/mus.10358

762